

X-ray absorption of cold gas: Simulating interstellar molecular clouds in the laboratory

I. Gissis,^{*} A. Fisher,[†] and E. Behar[‡]

Physics Department, Technion, Israel Institute of Technology, Haifa 3200003, Israel

(Dated: June 18, 2021)

Galactic and extra-galactic sources produce X-rays that are often absorbed by molecules and atoms in giant molecular clouds (GMCs), which provides valuable information about their composition and physical state. We mimic this phenomenon with a laboratory Z-pinch X-ray source, which is impinging on neutral molecular gas. The novel technique produces a soft X-ray pseudo continuum using a pulsed-current generator. The absorbing gas is injected from a 1 cm long planar gas-puff without any window or vessel along the line of sight. An X-ray spectrometer with a resolving power of $\lambda/\Delta\lambda \sim 420$, comparable to that of astrophysical space instruments, records the absorbed spectra. This resolution clearly resolves the molecular lines from the atomic lines; therefore, motivating the search of molecular signature in astrophysical X-ray spectra. The experimental setup enables different gas compositions and column densities. K-shell spectra of CO₂, N₂ and O₂ reveal a plethora of absorption lines and photo-electric edges measured at molecular column densities between $\sim 10^{16} \text{ cm}^{-2}$ – 10^{18} cm^{-2} typical of GMCs. We find that the population of excited-states, contributing to the edge, increases with gas density.

I. INTRODUCTION

X-rays from X-ray binaries (XRBs) and active galactic nuclei (AGNs) are often absorbed in the interstellar (ISM) and intergalactic (IGM) media. Giant molecular clouds (GMC) are abundant in the ISM and in star-forming regions. One of the main questions relevant to GMCs is their chemistry and heating mechanism affected by X-rays, shock-waves and cosmic rays [1]. In X-ray dominated regions (XDR), the X-rays penetrate deep into the cloud, releasing secondary electrons, which heat, dissociate and further ionize the gas. IR and mm emission of molecular tracers provide temperature and composition diagnostics [2, 3] including for high red-shift AGNs [4]. Complementary diagnostics comes from high-resolution X-ray (0.3 – 10 keV) absorption [5] and fluorescence [6]. Thus, it is important to study the X-ray absorption of these tracers in the laboratory.

A. Laboratory molecular absorption

Near edge X-ray absorption fine structure (NEXAFS) is a common method to characterize the elemental composition of thin solid samples, by probing the fine absorption features near the photo-electric edge. NEXAFS is originally and routinely performed in large beam facilities, i.e. synchrotrons [7] or free electron lasers [8]. It is of high interest to various scientific disciplines such as the study of organic sheets [9], nanoscale samples [10], inorganic polymers [11], and astrophysical dust [12, 13]. Table-top NEXAFS systems that can carry out a large

volume of tests at a high repetition rate are therefore desirable. Laser produced plasma (LPP) is the leading technique [14]. However, table-top LPPs require hundreds of shots to obtain a single high SNR spectrum. We have developed the GLIDER [15], a compact pulsed-power X-ray source of $\sim 10^{17} \text{ ergs}^{-1}$, which enables the measurement of NEXAFS of any matter-phase in an individual $\sim 10 \text{ ns}$ shot and dozens of shots per hour. In this paper, we report on NEXAFS diagnostics of astrophysical molecules found in GMCs.

II. EXPERIMENTAL SETUP AND METHODOLOGY

The experimental setup is depicted in Figure 1. A gas-puff Z-pinch plasma X-ray source is produced using the GLIDER generator [15]. The Z-pinch source is optimized for absorption measurements of the CNO K-shell spectral range (20 – 50 Å) by using imploding Kr gas. Unlike low-Z elements, Kr has a multitude of blended M-shell lines which produce a pseudo continuum soft X-ray and UV back-lighter to be absorbed by the CNO gas. The absorbing gas is injected through a second gas-puff along the line of sight, $\sim 300 \text{ mm}$ away from the pinch, and decoupled from it. The gas-puff injector is fast enough to prevent interaction between the absorber and the source. A reflection grating spectrometer (RGS) combined with a gated micro channel plate (MCP) detector records the absorption spectrum. Importantly, we avoid polymers such as polyimide or mylar windows, for they comprise C, N and O, which absorb strongly in the spectral range of interest. Indeed, our high resolution spectra of polyimide revealed significant C NEXAFS features. To avoid ambiguous diagnostics and to still protect the grating from debris and stray light, a glass capillary array is placed between the gas absorber and the grating entrance slit.

^{*} itaigiss@gmail.com

[†] amnon.fisher@gmail.com

[‡] behar@physics.technion.ac.il

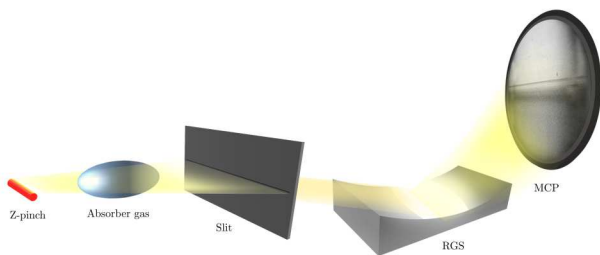


FIG. 1. Schematic experimental setup.

A. Wavelength calibration

Wavelength calibration was achieved using accurately known emission lines of highly ionized K-shell C, N and O in dedicated Z-pinch shots with no absorber. To calibrate the O K-edge around 23 Å, the resonance lines of $N^{+5,+6}$ and $O^{+6,+7}$ are used. To calibrate the N K-edge around 31 Å the resonant lines of $C^{+4,+5}$ and $N^{+5,+6}$ are used. The C K-edge around 42 Å region was calibrated using both 1st order diffraction C lines, e.g. at 33.736 (Ly α), 40.2678 (He α), 34.973 (He β) and 2nd order O lines, e.g. at 37.9340 (Ly α), 43.202 (He α). Each ~ 10 Å range is calibrated using 5–10 peaks resulting in systematic wavelength uncertainty of ≤ 7 mÅ. The spectrometer alignment is sensitive to temperature fluctuations. Therefore, spectral calibration was performed within minutes before or after the absorption shots.

B. Transmission spectral modeling

Transmission spectra are obtained by dividing an absorbed spectrum by one in a separate shot, which is unabsorbed in the range of interest. The transmission is defined as $e^{-\tau}$, where τ is the optical depth. The column density N of the absorber is related to the optical depth through: $\tau = N\sigma$ where, $\sigma(\lambda)$ is the cross-section profile for absorption in a spectral line or an edge. Column densities are estimated by dividing the measured $\tau(\lambda)$ by the published $\sigma(\lambda)$ [16]. The column density is also: $N = \int n(l) dl$, where $n(l)$ is the number density along the line of sight and is measured independently as described in Section III B.

Each NEXAFS is modeled with a single edge and several resolved lines. The edge is modeled with a λ^3 profile (hydrogenic approximation) and the lines are modeled as Gaussians with fitted widths. Since we did not observe ionized or highly excited states, we assume all molecules are in their electronic ground-state, but could be vibrationally or rotationally excited. These excitations may be reflected in the absorption lines, but the edge still manifests the total molecular column density. The entire model was further convoluted with a Gaussian of $\sigma = 50 - 70$ mÅ accounting for the instrumental broadening. The data are fitted using NASA's Xspec spectral

analysis code [17].

III. RESULTS

In Figure 2 we present normalized NEXAFS spectra of CO_2 , N_2 and O_2 . The models capture all main features identified in the literature to within ~ 1 eV. The results are summarized in Tables I, II, and III. The molecular neutral K α and the edge is clearly resolved in all three spectra. No ionized spectral lines are found short-ward of the edge. In C and N the neutral atom K α is resolved and is ~ 10 times weaker than the molecular K α . Hence, the molecules are essentially neutral and only mildly dissociated.

A few exceptional details are worth noting: The molecular K α in all CO_2 shots is split into two peaks (No. 2 and 3 in Figure 2). The mean peak value is 42.63 Å, consistent with the $(2\sigma_g)^{-1}2\pi_u$ transition [16, Figure 4.2.5 therein]. The deep feature at 39.8 Å (No. 9) dominates the edge as it does in [18]. The edge starts at 41.84 Å and its recovery is seen shortward of 39 Å.

In N_2 as well, almost all the absorption features fit their tabulated positions to within ~ 1 eV. An exception is the edge, which is measured here ~ 3 eV above the value in [16]. This is likely due to blending of the edge with the strong double-excitation feature at ~ 413 eV [16, Figure 3.2.6 therein].

In O_2 the K α resonance comprises a few transitions. We fit it with two blended peaks at 23.37 Å, A broad one (No. 1 in Figure 2) and a narrow one (No. 2). Unlike N_2 and CO_2 , in O_2 the atomic O K α at ~ 527 eV [22] is absent and likely obscured by the broad No. 1 feature. Our confidence in the O_2 interpretation is lower than in N_2 or CO_2 for the Kr emission in this energy range is not as smooth, and residual Kr emission may linger in the transmission spectrum.

TABLE I. CO_2 absorption lines and photo-electric edge around the C K-edge and their 1σ confidence interval.

| No. | Central wavelength Å | Central energy eV | Literature eV | Assignment |
|-----|-------------------------|-----------------------|------------------------|-----------------------------|
| 1 | $43.15^{+0.02}_{-0.01}$ | $287.4^{+0.1}_{-0.3}$ | 285 ^a | $1s2s^22p$ |
| 2 | $42.72^{+0.02}_{-0.01}$ | $290.3^{+0.1}_{-0.3}$ | | |
| 3 | $42.58^{+0.02}_{-0.01}$ | $291.3^{+0.1}_{-0.1}$ | 290.77 ^b | $(2\sigma_g)^{-1}2\pi_u$ |
| 4 | $42.33^{+0.02}_{-0.01}$ | $293.0^{+0.1}_{-0.1}$ | 292.74 ^b | $(2\sigma_g)^{-1}5\sigma_g$ |
| 5 | $42.02^{+0.01}_{-0.01}$ | $295.1^{+0.1}_{-0.1}$ | 295 ^c | $3p$ |
| 6 | $41.84^{+0.01}_{-0.02}$ | $296.4^{+0.1}_{-0.1}$ | 297.6 ^c | IP |
| 7 | $41.19^{+0.01}_{-0.02}$ | $301.1^{+0.1}_{-0.1}$ | 300.5–301 ^c | shake-up |
| 8 | $40.85^{+0.01}_{-0.04}$ | $303.6^{+0.2}_{-0.1}$ | 304.2 ^c | shake-up |
| 9 | $39.83^{+0.01}_{-0.04}$ | $311.4^{+0.2}_{-0.1}$ | 311–314 ^{b,c} | shake-up ^d |

^a Ref.[19] - mean value for all transitions

^b Ref.[16]

^c Ref.[18]

^d Blended with σ^* shape-resonance

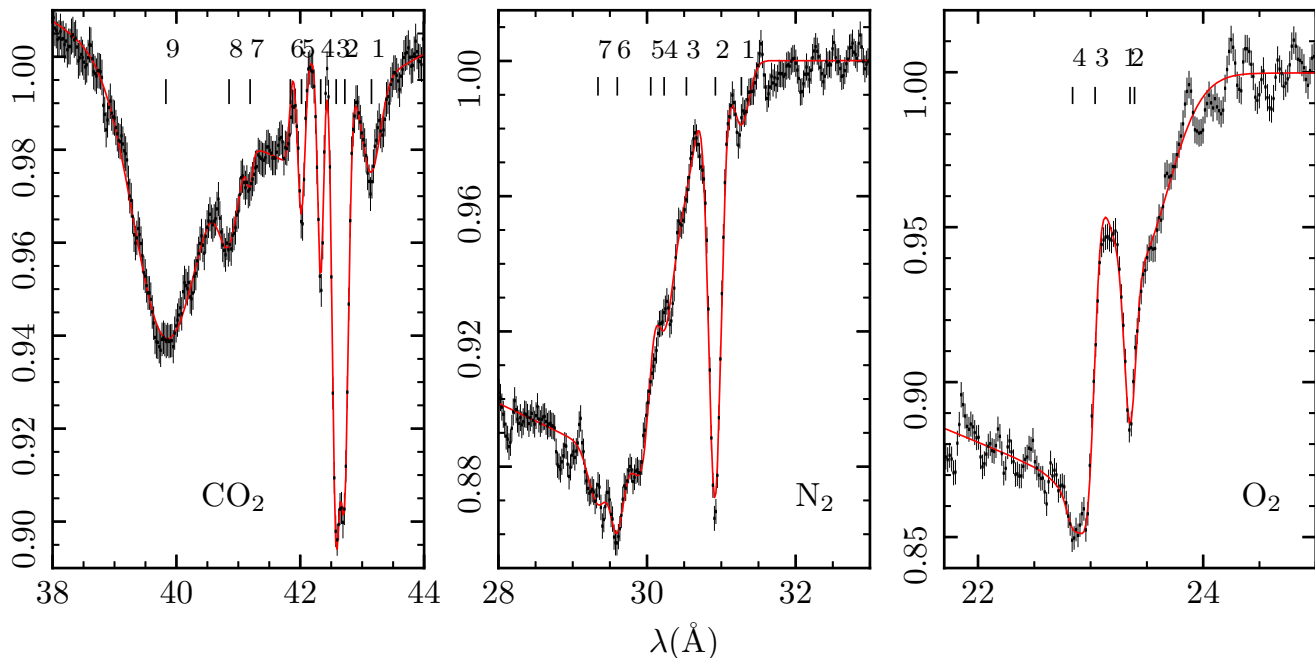


FIG. 2. Transmission spectra of CO₂ (C edge), N₂ and O₂ over a Kr back-lighter. The best fit model is plotted in solid red. The resolved transitions are marked on the figure and detailed in Tables I,II and III.

A. Column density measurements

For the sample spectra of Figure 2 we obtained 1.2 ± 0.1 , 10 ± 2 , 11 ± 2 in units of 10^{16} cm^{-2} for the CNO edges. This 10%–20% uncertainty is attributed to the fitting process of the $\sigma(\lambda)$ profile to the measured $\tau(\lambda)$.

A significant advantage of our experiment is the flexibility to control the absorber density and therefore the column density. In Figure 3 we present a set of experiments with N₂ at different initial plenum pressures. It can be seen from the figure that all NEXAFS features deepen as the pressure (and density) is increased.

TABLE II. Measured N₂ absorption lines and photo-electric edge and their 1σ confidence interval.

| No. | λ Å | E eV | Literature eV | Assignment |
|-----|-------------------------|-----------------------|---------------------|-------------------|
| 1 | $31.27^{+0.02}_{-0.01}$ | $396.6^{+0.2}_{-0.3}$ | 396 ^a | 1s |
| 2 | $30.92^{+0.02}_{-0.01}$ | $401.1^{+0.2}_{-0.2}$ | 400.96 ^b | $2p\pi_g(\pi^*)$ |
| 3 | $30.53^{+0.02}_{-0.02}$ | $406.2^{+0.2}_{-0.2}$ | 406.13 ^b | $3s\sigma_g$ |
| 4 | $30.23^{+0.01}_{-0.02}$ | $410.3^{+0.2}_{-0.2}$ | 408.36 ^b | $4s\sigma_g/3d$ |
| 5 | $30.05^{+0.01}_{-0.02}$ | $412.8^{+0.2}_{-0.2}$ | 413 ^c | Double excitation |
| | | | 409.9 ^c | IP |
| 6 | $29.60^{+0.01}_{-0.02}$ | $419.0^{+0.2}_{-0.2}$ | 418.9 ^b | $\sigma_u, l = 3$ |
| 7 | $29.34^{+0.01}_{-0.02}$ | $422.7^{+0.3}_{-0.2}$ | 421 ^b | shake-up |

^a Ref.[20]

^b Ref.[21]

^c Ref.[16]

The measured N₂ column densities are presented in Figure 4 as a function of the pressure, separately for the K α resonance (blue diamonds) and the edge (red circles). The values deduced from the edge are consistently higher than those deduced by the line. This ratio gradually increases with the plenum pressure. The N₂ edge cross-section is enhanced by additional features of excited molecules [16, Figure 3.2.6 therein]. This increases the opacity at the edge and thus, the deduced column density by more than a factor of 2. The remaining discrepancy between the edge and the line column density could be explained by the lines being absorbed only by ground-state molecules, while the edge is produced also by excited molecules in the ground configuration, and this excitation increases with pressure. Supporting evidence is the strong shake-up features measured in both

TABLE III. O₂ absorption lines and photo-electric edge and their 1σ confidence interval.

| No. | λ Å | E eV | Literature eV | Assignment |
|-----|-------------------------|-----------------------|--------------------|------------|
| 1 | $23.39^{+0.02}_{-0.01}$ | $530.3^{+0.2}_{-0.5}$ | | |
| 2 | $23.35^{+0.02}_{-0.01}$ | $531.0^{+0.2}_{-0.2}$ | 530.8 ^a | π^* |
| 3 | $23.04^{+0.01}_{-0.01}$ | $538.3^{+0.2}_{-0.2}$ | $\sim 540.5^b$ | IP |
| 4 | $22.84^{+0.01}_{-0.03}$ | $543.0^{+0.4}_{-0.2}$ | 539.3 ^b | σ^* |

^a Ref.[21]. Lines 1 and 2 are blended, while line 1 is broadened (Figure 2).

^b Ref.[16]. We measure a broad σ^* shape-resonance, next to the edge.

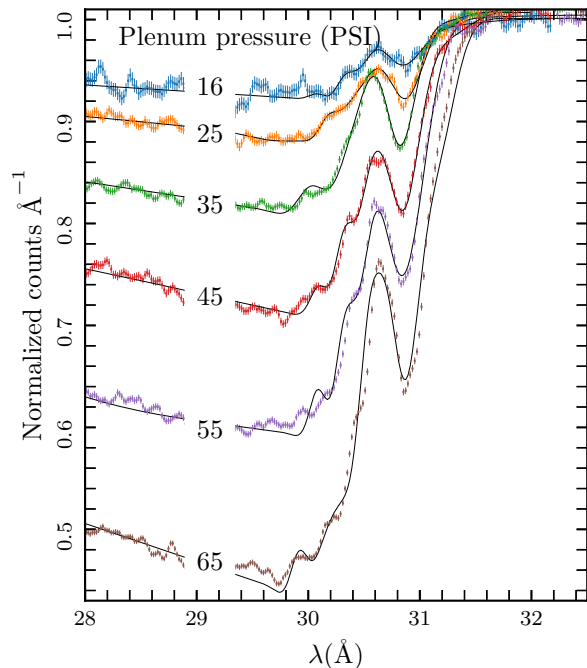


FIG. 3. Spectra of N_2 absorber on a Kr pinch background. The absorber puff plenum pressure in each shot is written on its corresponding spectrum.

CO_2 and N_2 (See Tables I, II) following the X-ray and UV excitation, which requires a broad-band source similar to astrophysical sources.

The lack of significant heating and dissociation resembles less an XDR and more a remote GMC. This may be due to the relatively short X-ray pulse of ~ 10 ns, compared to the long dissociation times of $\sim \mu s$. The preceding UV pulse is also short, ~ 30 ns. The dissociation time $t_{\text{diss}} = (F\sigma)^{-1}$, where $F = 10^{23} \text{ ph s}^{-1} \text{ cm}^{-2}$ is the measured photon flux above 10 eV [15]. The cross-section is $\sigma = 10^{-18} - 10^{-16} \text{ cm}^2$ varying over the spectral band [23], which results in $t_{\text{diss}} = 0.1 - 10 \mu s$.

B. Independent density measurement

The pressure of the absorber was measured independently with a piezo-electric gauge, located downstream from the absorber puff nozzle exit, at the vertical position of the spectrometer slit. The gauge measures the stagnation pressure which has a fixed ratio to the isentropic pressure and to the number density. The column density is this number density times the known planar nozzle length of 1 cm. The deduced gas column density is plotted in Figure 4 as the black crosses. The agreement between the spectroscopically deduced column densities and the gauge measurement enhances our confidence in the cross-sections used, albeit the experimental uncertainties.

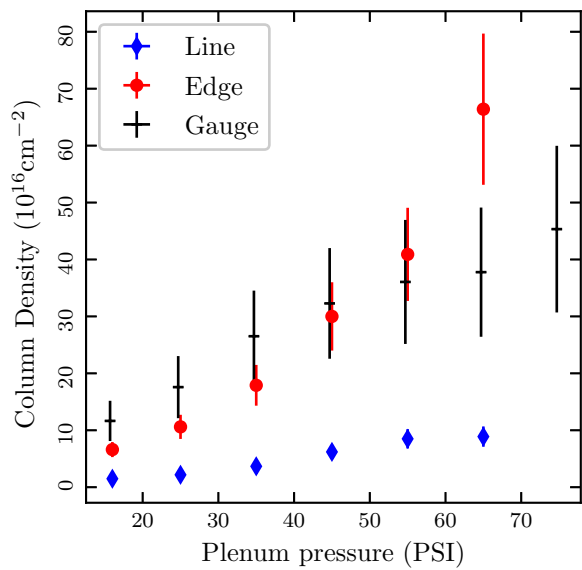


FIG. 4. Column density as a function of the absorber puff plenum pressure. Measurements are based on the line, edge and a piezo-electric pressure gauge. The column density uncertainties reflect also the variance between shots.

Beyond the 10%–20% uncertainty in the column density measured in an individual shot, the transmission spectra (Figures 2 and 3) vary from shot to shot by $\sim 15\%$. These variations between shots stem from the imperfect mechanics of the absorber puff, and are reflected in the error bars in Figure 4. The gauge density uncertainty results from the statistical repeatability of the injected gas density and the gauge SNR. All sum up to 30% uncertainty.

IV. CONCLUSIONS

We present a novel experiment to measure X-ray absorption by gaseous abundant molecules and atoms, mimicking astrophysical absorption in the ISM. This is the first time absorption of abundant astrophysical gases is measured with a pulsed-power X-ray source. We measured high resolution NEXAFS spectra of CO_2 , N_2 and O_2 , identifying numerous absorption lines. In the present experiment the gas is excited by a broad-band pseudo-continuum Kr Z-pinch source. Therefore, the absorber is photo-excited similarly to molecular clouds exposed to X-ray astrophysical sources. We demonstrate a wide dynamic range of absorber densities. Utilizing the X-ray astronomy fitting code Xspec, we deduced column densities of $\sim 10^{17} \text{ cm}^{-2}$, in good agreement with independently measured pressure.

The present setup opens the path for many more high-resolution X-ray absorption experiments that can support spectral interpretation of astrophysical sources and material science research. Improving the accuracy of the

independent density measurement will allow to benchmark excitation cross-sections. We are now preparing to integrate a second spectrometer and measure the absorbed and un-absorbed spectra simultaneously; thus, improving the accuracy of the NEXAFS spectrum. We are currently extending our measurements to photo-

ionized atomic species, also abundant in the ISM.

ACKNOWLEDGMENTS

We acknowledge support by the Center of Excellence of the ISF (grant No. 2752/19), and a grant from the Pazy Foundation. We thank S. Bialy for useful comments on the manuscript.

-
- [1] R. Meijerink and M. Spaans, Diagnostics of irradiated gas in galaxy nuclei. I. A far-ultraviolet and X-ray dominated region code, *Astronomy and Astrophysics* **436**, 397 (2005), arXiv:astro-ph/0502454 [astro-ph].
- [2] A. G. G. M. Tielens, The molecular universe, *Reviews of Modern Physics* **85**, 1021 (2013).
- [3] P. R. Maloney, D. J. Hollenbach, and A. G. G. M. Tielens, X-Ray-irradiated Molecular Gas. I. Physical Processes and General Results, *The Astrophysical Journal* **466**, 561 (1996).
- [4] L. Vallini, A. Pallottini, A. Ferrara, S. Gallerani, E. Sobacchi, and C. Behrens, CO line emission from galaxies in the Epoch of Reionization, *Monthly notices of the royal astronomical society* **473**, 271 (2018), arXiv:1709.03993 [astro-ph.GA].
- [5] K. Joachimi, E. Gatuzz, J. A. García, and T. R. Kallman, On the detectability of CO molecules in the interstellar medium via X-ray spectroscopy, *Monthly notices of the royal astronomical society* **461**, 352 (2016), arXiv:1606.02285 [astro-ph.HE].
- [6] T. Kawamuro, T. Izumi, K. Onishi, M. Imanishi, D. D. Nguyen, and S. Baba, AGN X-Ray Irradiation of CO Gas in NGC 2110 Revealed by Chandra and ALMA, *The Astrophysical Journal* **895**, 135 (2020), arXiv:2004.09394 [astro-ph.GA].
- [7] B. M. Kincaid and P. Eisenberger, Synchrotron radiation studies of the k -edge photoabsorption spectra of kr , br_2 , and gecl_4 : A comparison of theory and experiment, *Phys. Rev. Lett.* **34**, 1361 (1975).
- [8] H. Iwayama, M. Nagasaka, I. Inoue, S. Owada, M. Yabashi, and J. R. Harries, Demonstration of transmission mode soft x-ray nexafs using third- and fifth-order harmonics of fel radiation at sacra bl1, *Applied Sciences* **10**, 10.3390/app10217852 (2020).
- [9] G. Hähner, Near edge x-ray absorption fine structure spectroscopy as a tool to probe electronic and structural properties of thin organic films and liquids, *Chem. Soc. Rev.* **35**, 1244 (2006).
- [10] T. Hemraj-Benny, S. Banerjee, S. Sambasivan, M. Balasubramanian, D. Fischer, G. Eres, A. Puretzky, D. Geohagan, D. Lowndes, W. Han, J. Misewich, and S. Wong, Near-edge x-ray absorption fine structure spectroscopy as a tool for investigating nanomaterials, *Small* **2**, 26 (2006), <https://onlinelibrary.wiley.com/doi/pdf/10.1002/sml.200500256>.
- [11] O. Dhez, H. Ade, and S. Urquhart, Calibrated nexafs spectra of some common polymers, *Journal of Electron Spectroscopy and Related Phenomena* **128**, 85 (2003).
- [12] E. Costantini, S. T. Zeegers, D. Rogantini, C. P. de Vries, A. G. G. M. Tielens, and L. B. F. M. Waters, X-ray extinction from interstellar dust. Prospects of observing carbon, sulfur, and other trace elements, *Astronomy and Astrophysics* **629**, A78 (2019), arXiv:1906.08653 [astro-ph.GA].
- [13] J. C. Lee, J. Xiang, B. Ravel, J. Kortright, and K. Flanagan, CONDENSED MATTER ASTROPHYSICS: A PRESCRIPTION FOR DETERMINING THE SPECIES-SPECIFIC COMPOSITION AND QUANTITY OF INTERSTELLAR DUST USING X-RAYS, *The Astrophysical Journal* **702**, 970 (2009).
- [14] P. Wachulak, M. Duda, A. Bartnik, A. Sarzyński, L. Wegrzyński, M. Nowak, A. Jancarek, and H. Fiedorowicz, Compact system for near edge x-ray fine structure (nexafs) spectroscopy using a laser-plasma light source, *Opt. Express* **26**, 8260 (2018).
- [15] I. Gissis, E. Behar, A. Fisher, S. Aricha, E. Yeger, U. Avni, and I. Schnitzer, Glider—a pulsed-current generator for laboratory astrophysics x-ray absorption experiments, *Review of Scientific Instruments* **91**, 024701 (2020), <https://doi.org/10.1063/1.5133056>.
- [16] J. Berkowitz, *Atomic and Molecular Photoabsorption: Absolute Part* (Elsevier Science, 2015).
- [17] K. A. Arnaud, Astronomical data analysis software and systems v, *ASP Conf. Series* **101**, 11 (1996).
- [18] T. K. Sham, B. X. Yang, J. Kirz, and J. S. Tse, K -edge near-edge x-ray-absorption fine structure of oxygen- and carbon-containing molecules in the gas phase, *Phys. Rev. A* **40**, 652 (1989).
- [19] M. F. Hasoglu, S. A. Abdel-Naby, T. W. Gorczyca, J. J. Drake, and B. M. McLaughlin, K-SHELL PHOTOABSORPTION STUDIES OF THE CARBON ISONUCLEAR SEQUENCE, *The Astrophysical Journal* **724**, 1296 (2010).
- [20] J. García, T. R. Kallman, M. Witthoeft, E. Behar, C. Mendoza, P. Palmeri, P. Quinet, M. A. Bautista, and M. Klapisch, Nitrogen k -shell photoabsorption, *The Astrophysical Journal Supplement Series* **185**, 477 (2009).
- [21] A. Hitchcock and C. Brion, K -shell excitation spectra of co , n_2 and o_2 , *Journal of Electron Spectroscopy and Related Phenomena* **18**, 1 (1978).
- [22] B. M. McLaughlin, C. P. Ballance, K. P. Bowen, D. J. Gardenghi, and W. C. Stolte, HIGH PRECISION k -SHELL PHOTOABSORPTION CROSS SECTIONS FOR ATOMIC OXYGEN: EXPERIMENT AND THEORY, *The Astrophysical Journal* **771**, L8 (2013).
- [23] W. Huebner and J. Mukherjee, Photoionization and photoionization rates in solar and blackbody radiation fields, *Planetary and Space Science* **106**, 11 (2015).